Modeling seismic attenuation due to wave-induced fluid flow in the mesoscopic scale to interpret laboratory measurements

Beatriz Quintal and Nicola Tisato, ETH Zurich, Switzerland

Abstract

We measured seismic attenuation in the frequency range from 1 to 100 Hz and transient fluid pressure in partially saturated Berea sandstone. The sample was saturated with 97% water (3% air). To test whether fluid flow in the mesoscopic scale was the main cause of the measured attenuation, we performed numerical modeling to compute attenuation and transient fluid pressure on a 3D poroelastic model that represents the partially saturated sample. Wave-induced fluid flow in the mesoscopic scale was the only attenuation mechanism accounted for in the numerical solution. The numerical results reproduced the laboratory data for transient fluid pressure. The numerically calculated attenuation, superposed to the frequency-independent attenuation measured in the dry rock, reproduced attenuation measured in the partially saturated sample. These results show that wave-induced fluid flow in the mesoscopic scale is the dominant mechanism for the frequency-dependent component of seismic attenuation in partially saturated sandstone.

Introduction

Attenuation of seismic waves is a subject that has received increasing attention in the last decades. This is probably associated to an increasing amount of laboratory and field data showing that partially saturated rocks, such as hydrocarbon reservoirs, commonly exhibit high and frequency-dependent attenuation at seismic frequencies (e.g., Korneev et al 2004; Tisato and Madonna 2012). In this study, we combine numerical modeling and laboratory measurements to better understand the physical mechanisms controlling seismic attenuation in partially saturated rocks.

The laboratory experiments are performed using the Broad Band Attenuation Vessel (BBAV, Tisato and Madonna 2012), a machine designed to measure extensional-mode attenuation at seismic frequencies (0.1-100 Hz) in fluid-saturated rock samples. In addition to attenuation, we also measure the transient fluid pressure caused by a quick variation of the compressional stress applied on top of the sample. The transient fluid pressure is measured at different positions in the fluid-saturated rock sample, with pressure sensors laterally introduced into the sample and vertically spaced by about 4.2 cm from each other. These measurements of transient fluid pressure are related to fluid pressure gradients in the mesoscopic scale, and therefore to fluid flow in such a scale. The mesoscopic scale is much larger than the pore size and much smaller than seismic wavelengths. Our aim is to verify if wave-induced fluid flow in the mesoscopic scale can explain the high amplitudes and frequency dependence of the measured seismic attenuation in our rock sample. For that, we numerically compute attenuation and fluid pressure associated to wave-induced fluid flow in the mesoscopic scale using a model which is analogous to the fluid-saturated rock sample used in the laboratory.

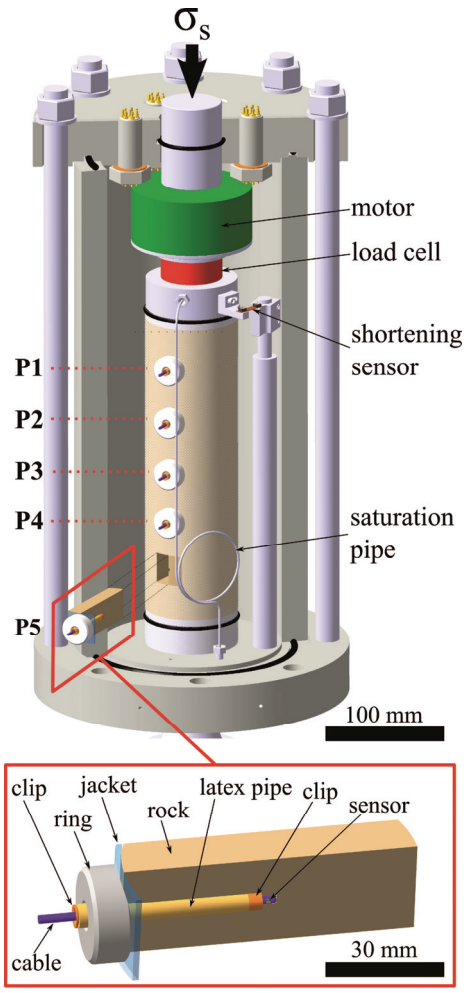

Figure 1. Sketch of the BBAV.

Wave-induced fluid flow in the mesoscopic scale is a physical mechanism that can yield such large attenuation at seismic frequencies in partially saturated porous media (Pride et al. 2004). In this physical mechanism, the passing seismic wave induces fluid pressure differences between regions having different compliances. These pressure gradients induce flow of viscous fluid and, therefore, part of the energy involved in the wave propagation is lost due to viscous dissipation. In partially saturated rocks, regions having different compliances occur due to heterogeneities in fluid saturation, accompanied or not by heterogeneities in the solid frame. In White's model (White 1975), a partially saturated rock is approximated by a medium with a homogeneous solid frame, heterogeneities fully saturated with one fluid, and the background fully saturated with another fluid (i.e., patchy saturation).

Dutta and Odé (1979a, b) showed that wave-induced fluid flow in the mesoscopic scale could be simulated using Biot's equations of wave propagation in poroelastic media (Biot 1962) with spatially varying petrophysical parameters. Numerical methodologies which are computationally efficient in calculating attenuation due to wave-induced fluid flow in the mesoscopic scale have been recently proposed by Masson and Pride (2007), Rubino et al. (2009), Wenzlau et al. (2010), and Quintal et al. (2011). These methodologies are based on quasi-static tests performed on poroelastic models. Quintal et al. (2011) proposed to solve Biot's equations for the consolidation (Biot 1941) of poroelastic media for such tests, rather than Biot's equations of wave propagation, as previously done. They solved Biot's equations of consolidation in the displacement-pressure formulation using the finite-element method (Zienkiewicz et al. 1999). We follow the methodology proposed by Quintal et al. (2011) to compute attenuation due to wave-induced fluid flow in the mesoscopic scale in a 3D numerical model.

Combining measurements of attenuation and fluid pressure, and using numerical modeling to assist in the interpretation of these data, allowed us to conclude that the amplitude and frequency dependence of seismic attenuation in partially saturated Berea sandstone samples can be explained by wave-induced fluid flow in the mesoscopic scale if the matrix anelasticity is taken into account.

Methodology

We use the BBAV (Figure 1, Tisato and Madonna 2012) to measure seismic attenuation in a partially saturated Berea sandstone sample in the frequency range from 1 to 100 Hz. The rock sample is cylindrical measuring 7.6 cm in diameter and 25 cm in length. Water saturation is increased (imbibition) from about 0% to about 97% by injecting water at the bottom of the sealed sample (undrained test). We also measure transient fluid pressure in the partially saturated sample. The transient fluid pressure is caused by a quick variation (approximately a step function) of the compressional stress applied on top of the sample. Five pressure sensors are laterally inserted into the sample, vertically spaced about 4.2 cm from each other (Figure 1). As the sensors were originally designed to measure intravascular blood pressure, holes of only few millimeters in diameter are drilled on sample. All measurements are performed at room temperature and pressure.

To compute attenuation due to wave-induced fluid flow in the mesoscopic scale, we employ a numerical methodology that was proposed by Quintal et al. (2011). We perform quasi-static creep tests on poroelastic models by numerically solving Biot's equations for the consolidation (Biot 1941) of poroelastic media. In our algorithm, these equations are used in the displacement-pressure formulation and solved with the finite-element method (Zienkiewicz et al. 1999). An undrained (no fluid flow at boundaries) boundary condition is mathematically fulfilled (natural boundary condition), which is possible due to the u-p formulation (e.g., equation B7 in Quintal et al. 2011). The algorithm was validated through comparison of numerical results with analytical solutions and it allows for stable and accurate results in a broad frequency range (Quintal et al. 2011, 2012). In order to solve our problem for a three-dimensional (3D) model, we here use the finite-element commercial software COMSOL Multiphysics, mainly due to its 3D mesh generator. We employ an unstructured mesh composed of tetrahedral elements.

The numerical model is cylindrical with the following boundary conditions: (i) An approximate step stress (time function) is applied on top of the model. (ii) The bottom is fixed (no displacement in the z direction). (iii) The sides are also fixed (no displacement in the x and y directions). Time-dependent normal total stress and strain in the z direction, σ_{zz} and ε_{zz}, are obtained from this experiment. Subsequently, a first-time derivative is applied to them resulting in the stress and strain rates. The rates are converted into the frequency domain with a fast Fourier transform, resulting in T_{zz} and S_{zz}. Finally, the complex and frequency-dependent P-wave modulus is calculated as

$$H(\omega) = \frac{T_{zz}}{S_{zz}}, \tag{1}$$

from which the frequency-dependent Young's modulus can be calculated,

$$E(\omega) = \frac{\mu(3H - 4\mu)}{H - \mu}, \tag{2}$$

where ω is the angular frequency and μ is the shear modulus of the saturated medium. We then calculate attenuation as

$$Q^{-1}(\omega) = \frac{\mathrm{Im}(E)}{\mathrm{Re}(E)}, \tag{3}$$

referred to as extensional-mode attenuation (same type is obtained in the laboratory).

Results

The numerical model has the same dimensions as the Berea sandstone sample used in the laboratory. Because Berea sandstone has a solid frame which can be considered homogeneous at mesoscopic scales, heterogeneities only in fluid saturation are implemented in the numerical model. According to Gassmann's

equations, the shear modulus of the saturated medium (used in equation 2) is equal to the shear modulus of the dry frame when the solid frame is homogeneous (Gassmann 1951; Berryman 1999). The petrophysical properties for the solid frame are given in Table 1. For the saturation in the model, properties of water and air are listed in Table 2. The objective is to compare numerical results with laboratory data for the case in which the rock sample is saturated with 97% water.

Table 1. Physical properties of the solid frame.

Rock	Sandstone
Bulk modulus of the grains (GPa)	36
Porosity (%)	20
Permeability (mD)	300
Bulk modulus of the dry frame (GPa)	7
Shear modulus of the dry frame (GPa)	4.8

Table 2. Physical properties of the fluids.

Fluid	Water	Air
Viscosity (Pa·s)	0.001	2×10^{-5}
Bulk modulus (GPa)	2.2	10^{-4}

Figure 2. Numerical model.

As a first step to obtain the fluid distribution in the model, we use the laboratory data for fluid pressure at a time very close to zero (i.e., immediately after the application of the step stress) at the five locations along the sample. These values of fluid pressure suggest that water saturation is higher in the bottom of the sample, which is in agreement with the experimental setup since water is injected in the sample at the bottom. At a time very close to zero, sample parts saturated with an "incompressible" and viscous fluid (i.e., water) experiences a much higher fluid pressure than parts saturated with a gas (i.e., air) because water has no time to migrate towards parts under lower fluid pressure. Next, a linear relationship between the measured values of fluid pressure at a time very close to zero and water saturation is defined fixing the overall water saturation in the model to about the same as in the laboratory (97%). Following this linear relationship, we inserted air-saturated cubic patches in a fully-water saturated background to create models. Number and size of patches were increased toward the top of the model. The cubic shape was chosen because it is solved numerically using a small number of tetrahedral elements. To test if the saturation distribution was representative of the actual distribution in the sample, we compared transient fluid pressure obtained numerically and from laboratory measurements. The model shown in Figure 2 was chosen because it resulted in the best agreement between numerical and laboratory data for transient fluid pressure (Figure 3). A total of 120 cubic patches were employed, with sides measuring from 2 to 10 mm, yielding a total water saturation of about 98% in the model. From the same simulation that we obtained transient fluid pressure, we recorded the resulting time-dependent normal total stress and strain in the z direction and computed attenuation (Figure 4).

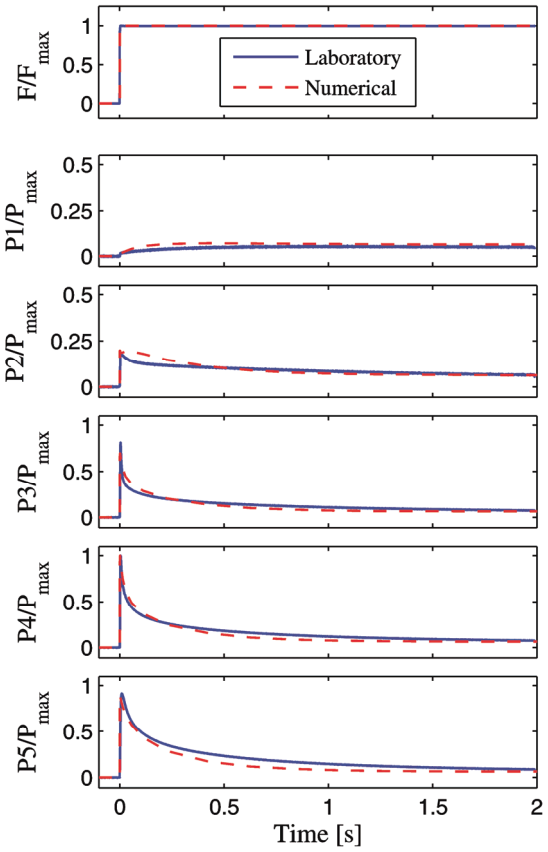

Figure 3. Laboratory and numerical results for transient fluid pressure.

The result of the numerical simulation is shown as the dashed red curve in Figure 4, and it accounts for attenuation only due to wave-induced fluid flow in the mesoscopic scale. However, in the laboratory data, also shown in Figure 4, we observe a non-negligible value of attenuation for the dry sample, approximately independent of frequency. Such attenuation associated to the solid frame is assumed to take place also in the measurements for the fluid-saturated sample (Johnston et al. 1979). To interpret laboratory data for attenuation in a fluid-saturated sample, Johnston et al. (1979) assumed that fluid-related attenuation ($1/Q_{\text{Fluid}}$) and frame-related attenuation ($1/Q_{\text{Frame}}$) are independent and that the total attenuation in the fluid-saturated rock could therefore be calculated as

$$\frac{1}{Q_{\text{Total}}} = \frac{1}{Q_{\text{Fluid}}} + \frac{1}{Q_{\text{Frame}}} . \qquad (4)$$

We follow the procedure used by Johnston et al. (1979) to interpret our laboratory measurements of attenuation in fluid-saturated rocks. The numerically calculated attenuation due to wave-induced fluid flow is taken as the value for $1/Q_{\text{Fluid}}$ and the mean value of laboratory measurements of attenuation in the dry sample, for $1/Q_{\text{Frame}}$. The sum ($1/Q_{\text{Total}}$) yields the black solid curve plotted in Figure 4 and is finally compared to the laboratory measurements of attenuation in the fluid-saturated sample. We observe that this curve fits relatively well the laboratory data. This shows that wave-induced fluid flow in the mesoscopic scale can explain the frequency-dependent compornent of seismic attenuation measured in partially saturated sandstone.

Discussion

Johnston et al. (1979) have shown for a series of datasets at ultrasonic frequencies that the overall attenuation of a rock may be considered to contain a frequency-independent component plus a frequency-dependent component. They assumed that the attenuation mechanisms were independent of each other and that the ones taking place in dry rocks also take place in saturated rocks. Measurements on dry and partially fluid-saturated rocks suggested that the frequency-independent component was due to matrix anelasticity and the frequency-dependent component was related to the fluid saturation. Matrix anelasticity includes the intrinsic (1) attenuation of matrix minerals and (2) aggregate minerals, in addition to (3) frictional dissipation due to relative motions at the grain boundaries and across crack surfaces (Walsh 1966; Johnston et al. 1979). The intrinsic attenuation of minerals is generally small ($Q^{-1} < 0.001$), while in the whole rock attenuation is normally much higher. For example, at room conditions, $Q^{-1} \sim 0.015$ for our dry sample. Thus, we assume that most of the attenuation measured in room-condition dry rocks is due to friction across grain boundaries and cracks and due to attenuation of the aggregate minerals. According to Walsh (1966), friction is probably the major factor when the dry samples are at room conditions. At room conditions certain amount of residual water will remain in many of the grain boundaries and thin cracks. A very thin layer of residual water (at least a mono-molecular layer) lubricates crack surfaces and favor sliding motions to take place even for low strains as the one used in our laboratory experiments, of the order 10-6. In the absence of water, such as under hard vacuum conditions, attenuation measured in rock samples is much lower (e.g., Tittmann et al. 1975) because no sliding motions can take place across surfaces (Johnston et al. 1979). Another case in which attenuation due to friction becomes negligible is when the rock is subjected to confining pressures high enough to close all cracks (Walsh 1966).

Because we study attenuation at seismic frequencies, that is, at frequencies lower than the range studied by Johnston et al. (1979), our interpretation for the frequency-dependent fluid-related attenuation is different than theirs. They concluded that Biot-type fluid flow mechanism (Biot 1962), although not necessarily dominating, plays an important role in the overall attenuation. However, at seismic frequencies, attenuation due to this mechanism is negligible for usual properties of fluid-saturated rocks (Bourbié et al. 1982). We considered wave-induced fluid flow in the mesoscopic scale to interpret our laboratory data and showed it can explain the frequency-dependent component of the data. If this mechanism, together with matrix anelasticity, is responsible for high values of attenuation ($Q^{-1} \sim 0.06$) at seismic frequencies, its occurrence in hydrocarbon reservoirs should be further investigated (e.g., Quintal 2012; Quintal et al. 2012).

Conclusion

We numerically modeled a creep test in a patchy saturated poroelastic model representing the partially saturated Berea sandstone used for laboratory experiments. The numerical results for attenuation, superposed to a constant attenuation due to the solid frame, reproduced fairly well the laboratory data. This demonstrates that wave-induced fluid flow in the mesoscopic scale is the dominant mechanism for the frequency-dependent component of seismic attenuation in partially saturated Berea sandstone.

Acknowledgments

This work was supported by the LFSP (Low Frequency Seismic Partnership) and the CTI (Swiss Commission for Technology and Innovation). We thank Holger Steeb for enlightening discussions, Claudio Madonna and Brad Artman for helping with the experimental design, Robert Hofmann and Reto Seifert for solving numerous technical problems. Luigi Burlini initiated the design of the BBAV but deceased in an early stage of the research.

References

Berryman, J. G., 1999, Origin of Gassmann's equations: Geophysics, 64, 1627-1629.

Biot, M. A., 1941, General theory of three-dimensional consolidation: Journal of Applied Physics, 12, 155-164.

Biot, M. A., 1962, Mechanics of deformation and acoustic propagation in porous media: Journal of Applied Physics, 33, 1482-1498.

Bourbié, T., Coussy, O. and Zinszner, B., 1987, Acoustics of porous media, Editions Technip.

Dutta, N. C. and Odé, H., 1979a, Attenuation and dispersion of compressional waves in fluid filled porous rocks with partial gas saturation (White model) – Part I: Biot theory: Geophysics, 44, 1777-1788.

Dutta, N. C. and Odé, H., 1979b, Attenuation and dispersion of compressional waves in fluid filled porous rocks with partial gas saturation (White model) – Part II: Results: Geophysics, 44, 1789-1805.

Gassmann, F., 1951, Über die Elastizität poröser Medien: Vierteljahreschrift der Naturforschenden Gesellschaft in Zürich, 96, 1-23.

Johnston, D. H., Toksoz, M. N. and Timur, A., 1979, Attenuation of seismic wave in dry and saturated rocks: II. Mechanisms: Geophysics, 44, 691-711.

Korneev, V. A., Goloshubin, G. M., Daley, T. M., and Silin, D. B., 2004, Seismic low-frequency effects in monitoring fluid-saturated reservoirs: Geophysics, 69, 522-532.

Masson, Y. J. and Pride, S. R., 2007, Poroelastic finite-difference modeling of seismic attenuation and dispersion due to mesoscopic-scale heterogeneity: Journal of Geophysical Research, 112, B03204.

Pride, S. R., Berryman, J. G. and Harris, J. M., 2004, Seismic attenuation due to wave-induced flow: Journal of Geophysical Research, 109, B01201.

Quintal, B., Steeb, H., Frehner, M. and Schmalholz, S. M., 2011, Quasi-static finite element modeling of seismic attenuation and dispersion due to wave-induced fluid flow in poroelastic media: Journal of Geophysical Research, 116, B01201.

Quintal, B., Steeb, H., Frehner, M., Schmalholz, S. M., and Saenger, E. H., 2012, Pore fluid effects on S-wave attenuation caused by wave-induced fluid flow: Geophysics, 77, L13-L23.

Quintal, B., 2012. Frequency-dependent attenuation as a potential indicator of oil saturation, Journal of Applied Geophysics, 82, 119-128.

Rubino, J. G., Ravazzoli, C. L. and Santos, J. E., 2009, Equivalent viscoelastic solids for heterogeneous fluid-saturated porous rocks: Geophysics, 74, N1-N13.

Tisato, N., and Madonna, C., 2012, Attenuation at low seismic frequencies in partially saturated rocks: Measurements and description of a new apparatus: Journal of Applied Geophysics, 86, 44-53.

Tittmann, R. B., Houseley, R. M. and Abdel-Gawad, M., 1975, Internal friction quality factor ≥3100 achieved in lunar rock 70215, 85: Abstracts of the Lunar and Planetary Science Conference, 6, 812-814.

Walsh, J. B., 1966, Seismic wave attenuation in rock due to friction: Journal of Geophysical Research, 71, 2591-2599.

Wenzlau, F., Altmann, J. B. and Müller, T. M., 2010, Anisotropic dispersion and attenuation due to wave-induced fluid flow: Quasi-static finite element modeling in poroelastic solids: Journal of Geophysical Research, 115, B07204.

White, J. E., 1975, Computed seismic speeds and attenuation in rocks with partial gas saturation: Geophysics, 40, 224–232.

Zienkiewicz, O. C., Chan, A. H. C., Pastor, M., Schrefler, B. A. and Shiomi, T., 1999, Computational Geomechanics With Special Reference to Earthquake Engineering, John Wiley.

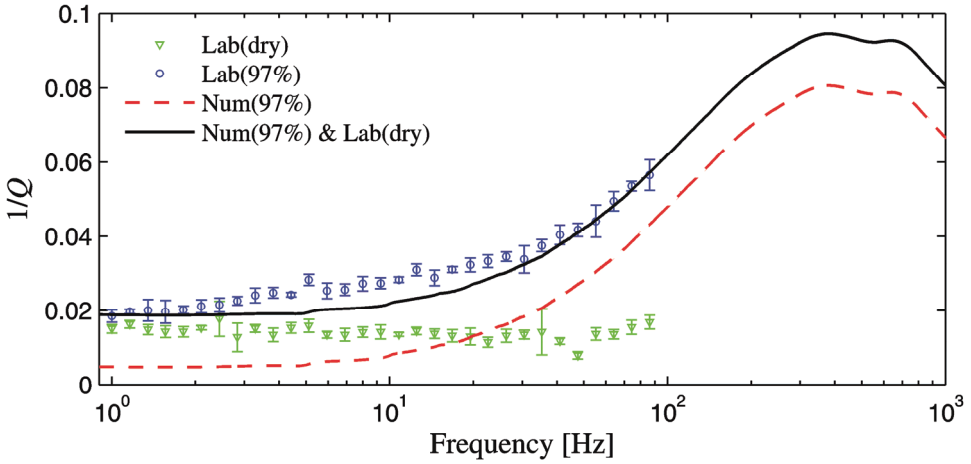

Figure 4. Laboratory and numerical results for attenuation.